CORE
Metadata, citation and similar papers at core.ac.uk
Provided by Elsevier - Publisher Connector

Cell

Intestinal Crypt Homeostasis Results from Neutral Competition between Symmetrically Dividing Lgr5 Stem Cells

Hugo J. Snippert,[1] Laurens G. van der Flier,[1] Toshiro Sato,[1] Johan H. van Es,[1] Maaike van den Born,[1] Carla Kroon-Veenboer,[1] Nick Barker,[1] Allon M. Klein,[2,3] Jacco van Rheenen,[1] Benjamin D. Simons,[3] and Hans Clevers[1,*]
[1]Hubrecht Institute, KNAW and University Medical Center Utrecht, Uppsalalaan 8, 3584 CT Utrecht, The Netherlands
[2]Department of Systems Biology, Harvard Medical School, 200 Longwood Avenue, Boston, MA 02115, USA
[3]Department of Physics, Cavendish Laboratory, J.J. Thomson Avenue, Cambridge CB3 0HE, UK
*Correspondence: h.clevers@hubrecht.eu
DOI 10.1016/j.cell.2010.09.016

SUMMARY

Intestinal stem cells, characterized by high *Lgr5* expression, reside between Paneth cells at the small intestinal crypt base and divide every day. We have carried out fate mapping of individual stem cells by generating a multicolor Cre-reporter. As a population, Lgr5^{hi} stem cells persist life-long, yet crypts drift toward clonality within a period of 1–6 months. We have collected short- and long-term clonal tracing data of individual Lgr5^{hi} cells. These reveal that most Lgr5^{hi} cell divisions occur symmetrically and do not support a model in which two daughter cells resulting from an Lgr5^{hi} cell division adopt divergent fates (i.e., one Lgr5^{hi} cell and one transit-amplifying [TA] cell per division). The cellular dynamics are consistent with a model in which the resident stem cells double their numbers each day and stochastically adopt stem or TA fates. Quantitative analysis shows that stem cell turnover follows a pattern of neutral drift dynamics.

INTRODUCTION

Although invertebrate stem cells and their niches can be studied with single-cell resolution, the size of mammalian tissues combined with the infrequent occurrence of stem cells have complicated the identification of individual stem cells in vivo (Morrison and Spradling, 2008). The small intestinal epithelium presents a unique opportunity to study mammalian adult stem cells. Not only is it the fastest self-renewing tissue in mammals, it also has a simple, highly stereotypical layout. It is essentially a two-dimensional (2D) structure: a sheet of cells, bent in space to form the crypts and villi. Cell compartments are easily identified by location along the crypt-villus axis. And, importantly, all cellular progeny remain associated with the stem cell compartment of origin. Stem cells reside at the crypt base and feed daughter cells into the TA compartment. TA cells undergo approximately 4–5 rounds of rapid cell division (Marshman et al., 2002). TA cells move out of the crypt and terminally differentiate into enterocytes, goblet cells, and enteroendocrine cells. These differentiated cells continue to move up the villus flanks to die upon reaching the villus tip after 2–3 more days. A fourth cell type, the Paneth cell, also derives from the stem cells but migrates downwards and settles at the crypt base to live for 6–8 weeks (van der Flier and Clevers, 2009).

Recently we reported that small cycling cells located between the Paneth cells, previously identified as crypt base columnar cells (Cheng and Leblond, 1974a, b), specifically express the *Lgr5* gene (Barker et al., 2007). Using lineage tracing, we demonstrated that these Lgr5^{hi} cells generate all cell types of the small intestinal epithelium throughout life. Similar data were obtained using a *CD133*-based lineage tracing strategy (Zhu et al., 2009). The Ascl2 transcription factor sets the fate of the Lgr5^{hi} cells (van der Flier et al., 2009). As further proof of stemness, single Lgr5^{hi} cells can generate ever-expanding epithelial organoids with all hallmarks of in vivo epithelial tissue (Sato et al., 2009). In the colon, stomach, and hair follicle, Lgr5^{hi} cells have also been identified as stem cells (Barker et al., 2007, Barker et al., 2010; Jaks et al., 2008), whereas the *Lgr6* gene marks a population of primitive skin stem cells (Snippert et al., 2010).

Previously it was postulated that a cycling, yet DNA label-retaining cell at position +4 represents a stem cell (Potten et al., 1974). Multiple markers were published for this cell (He et al., 2004, 2007; Potten et al., 2003). Using one of these markers, Bmi1, long-term lineage tracing was observed with kinetics that are surprisingly similar to that of Lgr5^{hi} cells (Sangiorgi and Capecchi, 2008). As sorted Lgr5^{hi} cells express the highest levels of *Bmi1* as assessed by qPCR analysis (Snippert et al., 2009; van der Flier et al., 2009), *Lgr5* and *Bmi1* may mark overlapping, if not identical, cell populations. Although a rare, quiescent "reserve" Lgr5^{neg} population may exist (Li and Clevers, 2010), the Lgr5^{hi} cells represent the workhorse of life-long self-renewal of the healthy small intestine.

The most popular view on how stem cell populations accomplish homeostasis involves asymmetric cell division, which—at the single stem cell level—results in two cells with unequal fates: one new stem cell and one TA cell. This pattern of "invariant asymmetry" in cell division can be controlled by cell-intrinsic mechanisms best exemplified by the first division of the

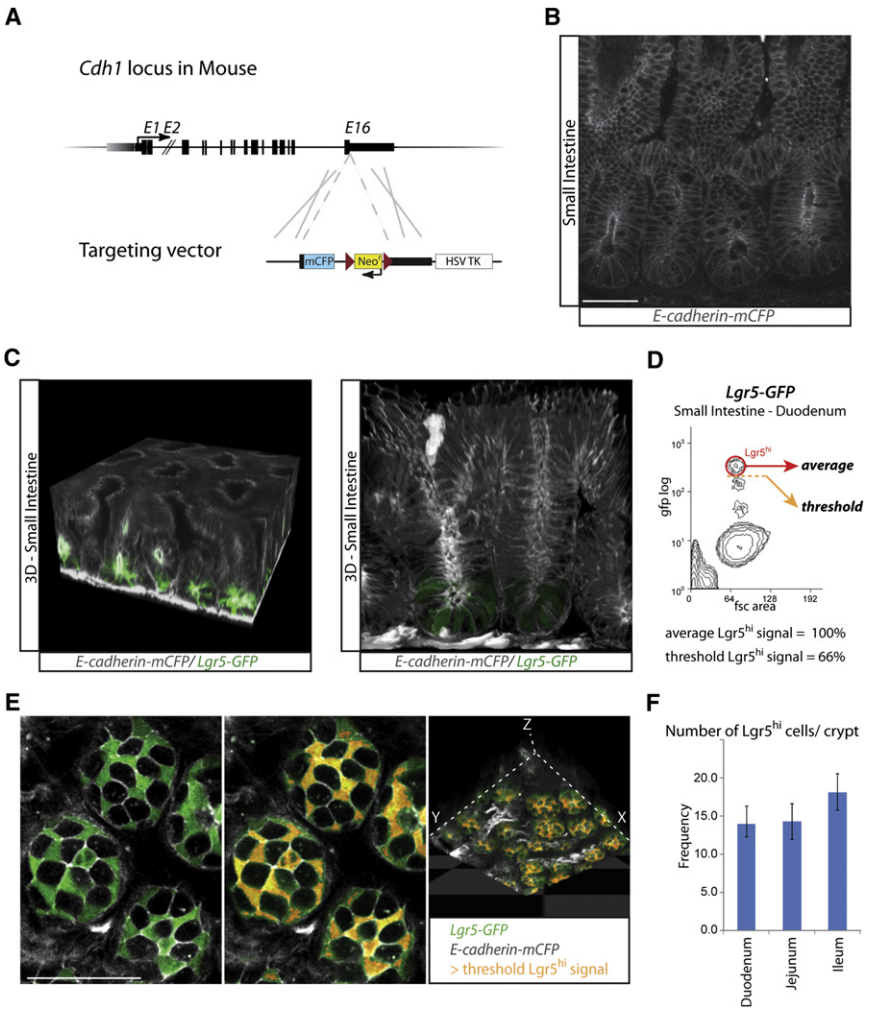

Figure 1. Location and Number of Lgr5^{hi} Cells per Crypt

(A) E-cadherin knock-in strategy in which the fluorescent protein monomer Cyan (mCFP) is fused to the C terminus of *Cdh1*.

(B) Cellular localization of E-cadherin-mCFP fusion protein (white) in crypts of small intestine.

(C) *E-cadherin-mCFP* mice crossed with *Lgr5-EGFP-Ires-CreERT2* mice. Left panel: whole-mount intestine scanned from crypt bottom to crypt-villus border (~125 μm); right panel: lateral scan of semi-thick section (~50 μm). E-cadherin-mCFP (white) allows 3D reconstruction of tissue architecture, whereas Lgr5-GFP (green) visualizes intestinal stem cells.

(D) FACS analysis of intestine of *Lgr5-EGFP-Ires-CreERT2* mice reveals three populations. GFP^{hi} represents Lgr5 intestinal stem cells.

(E) Whole-mount intestine from *E-cadherin-mCFP* (white)/*Lgr5-EGFP-Ires-CreERT2* (green) mice. Lgr5-GFP^{hi} population was visualized in red (false color), whereas E-cadherin-mCFP (white) marks cell borders. At the crypt base, all Lgr5^{+} cells were GFP^{hi}.

(F) Counting in 3D reconstructions yielded 14 ± 2 Lgr5^{hi} cells per crypt in proximal small intestine. Error bars represent standard deviation.

Scale bars: 50 μm. See also Figure S1.

C. elegans embryo (Cowan and Hyman, 2004) but also by extrinsic niche signals as shown for *Drosophila* germ stem cells (Fuller and Spradling, 2007). The asymmetric segregation of molecules coupled with strictly oriented mitotic spindles can herald an asymmetric fate outcome of the stem cell division, as shown for the *C. elegans* embryo and the *Drosophila* neuroblast (Neumuller and Knoblich, 2009). Only upon tissue expansion or damage will stem cells divide symmetrically in this model. We refer to mechanisms of stem cell maintenance that rely upon invariant asymmetry of division as belonging to the class of hierarchical models.

Another, less commonly considered model for homeostatic stem cell maintenance states that the two cells that are generated from a stem cell division do not necessarily display intrinsically divergent fates. Such a stem cell division can lead to any of three fate outcomes: two stem cells, one stem cell and one TA cell, or two TA cells. In order to maintain stem cell number in this model, homeostatic mechanisms have to act by necessity at the stem cell population level, ensuring that—on average—each stem cell division results in one stem cell and one TA cell. Stem cell-supported tissues that exhibit this pattern of regulatory control belong to the class of stochastic models. In contrast to hierarchical models, the clonal fate of individual stem cells in stochastic models is unpredictable.

Unlike most other mammalian tissues, the stem cells of the intestine are strictly compartmentalized in crypts. Winton and Ponder reported that the marking of individual stem cells results in entirely clonal crypts after 3 months and concluded that a single stem cell maintains each crypt (Winton and Ponder, 1990). Griffith et al. draw comparable conclusions for colonic crypts (Griffiths et al., 1988). In this view, crypt stem cell dynamics would represent an extreme version of the hierarchical model. Potten and Loeffler on the other hand proposed that crypts may harbor multiple stem cells that are not strictly dividing asymmetrically (Potten and Loeffler, 1990).

RESULTS

Lgr5^{hi} Cells Occur as a Homogeneous Population

Lgr5^{hi} stem cells in the small intestine divide approximately once per day (Barker et al., 2007). Quyn and colleagues have demonstrated that each Lgr5^{hi} stem cell orients its mitotic spindle along its apical-basal axis (Quyn et al., 2010). In order to visualize crypt architecture at single-cell resolution, we generated an *E-cadherin-mCFP* fusion knock-in allele (Figures 1A and 1B and Figure S1 available online) and crossed this into the *Lgr5-EGFP-Ires-CreERT2 KI* mouse strain. *E-cadherin-mCFP* mice were homozygous viable. The E-cadherin fusion protein allowed visualization of 3D crypt architecture to depths of 125 μm

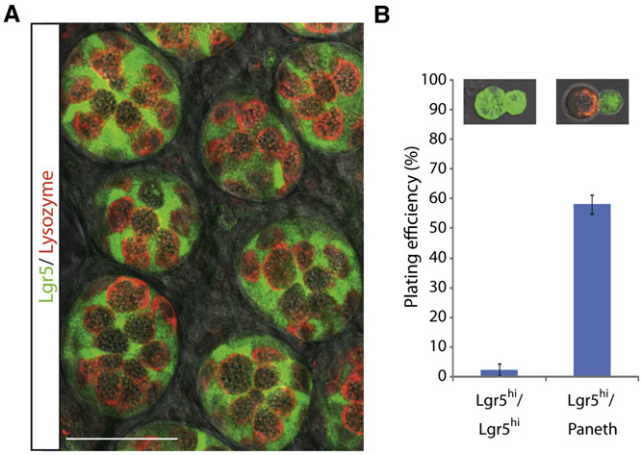

Figure 2. Lgr5^{hi} Cells Constitute an Equipotent Stem Cell Population

(A) Confocal section at the crypt base with Lgr5 cells (green) and Paneth cells, with large granules, stained for lysozyme (red). All cells at crypt bottoms are either Lgr5^{hi} cells or Paneth cells.

(B) Plating efficiency of Lgr5^{hi}/Lgr5^{hi} versus Lgr5^{hi}/Paneth doublets as scored after a 7 day culture shows outgrowth of ~60% of Lgr5^{hi} cells when paired with a Paneth cell. Insets: confirmation of sorting strategy by confocal microscopy; Lgr5^{hi} in green and Paneth cell in red. Error bars represent standard deviation. Scale bars: 50 μm.

(Figure 1C), which revealed an almost perfect intermingling of Lgr5^{hi} cells and Paneth cells (Figure 1E).

Fluorescence-activated cell sorting (FACS) analysis demonstrated the existence of three different Lgr5-expressing populations based on GFP level (Figure 1D), of which only the GFP^{hi} cells yield long-lived intestinal organoid structures in vitro (Sato et al., 2009). We next counted Lgr5^{hi} intestinal stem cells in duodenal crypts of *Lgr5-EGFP-Ires-CreERT2/E-cadherin-mCFP* mice. In the 3D reconstruction model (Figure 1E), essentially all non-Paneth cells at the crypt base were Lgr5-GFP^{hi}. Conversely, no Lgr5-GFP^{hi} cells were observed outside the crypt base. Crypts of the duodenum were found to contain 14 ± 2 Lgr5^{hi} cells (Figure 1F), similar to the numbers of crypt base columnar cells as originally reported (Cheng and Leblond, 1974b).

In our initial in vitro experiments, less than 5% of single sorted Lgr5 intestinal stem cells could grow out into gut-like organoid structures (Sato et al., 2009). Recently, we noted that sorted heterotypic doublets (consisting of one Lgr5^{hi} stem cell and one Paneth cell) displayed 25% plating efficiency (H.C. and T.S., unpublished data). After further optimization, we reached a plating efficiency of approximately 60% when scored as exponentially growing organoids after 7 days (Figure 2). In other words, more than half of Lgr5^{hi} cells could grow out into an intestinal organoid when sorted together with a neighboring Paneth cell. We interpreted this to imply that the majority of Lgr5^{hi} cells have stem cell properties, at least when associated with a Paneth cell. Thus, we tentatively viewed each duodenal crypt to harbor a homogeneous population of 14 Lgr5^{hi} intestinal stem cells.

Multicolor Lineage Tracing of Individual Lgr5 Stem Cells

To address how homeostatic self-renewal is controlled, we generated a Cre-reporter allele termed *R26R-Confetti*. We integrated into the *Rosa26* locus a construct consisting of the strong CAGG promoter, a LoxP-flanked Neo^{R}-cassette serving as transcriptional roadblock, and the original Brainbow-2.1 cassette (Livet et al., 2007) (Figure 3A). After Cre-mediated recombination, the roadblock was removed and one of the four fluorescent marker proteins was stochastically placed under control of the CAGG promoter, allowing discrimination between the clonal progeny of neighboring stem cells within the same niche (Figure 3B). We validated fluorescent expression in multiple organs using the β-naphtaflavone (bNF)-inducible *Ah-Cre* allele (Ireland et al., 2004). Cre induction in small intestinal crypts occurs at high efficiency, whereas less efficient induction of the Cre transgene occurs in a variety of other organs. The *R26R-Confetti* allele behaved as a stochastic multicolor Cre-reporter generating nuclear green, cytoplasmic yellow, cytoplasmic red, or membrane-bound blue cells (Figure 3C). Whereas the other three colors consistently appeared in near-equal ratios, nuclear GFP cells occurred at varying frequencies, yet always lower than the expected 25%.

Short-Term Clonal Tracing Analysis of Individually Labeled Lgr5^{hi} Cells

Crypts drift toward clonality over time (Griffiths et al., 1988; Winton and Ponder, 1990), yet the kinetics of this process have not been documented at the single stem cell level. In the first of two tracing strategies addressing this issue, we analyzed the behavior of clones developing from single Lgr5^{hi} cells, stochastically initiated using the *Lgr5-EGFP-Ires-CreERT2* allele in conjunction with the *R26R-Confetti* reporter. Analysis of stem cell clones was performed at various time points after Cre-activation by tamoxifen in 10-week-old mice, after which the progeny of these Lgr5^{hi} cells were mapped in 3D-reconstructed crypts. Labeling occurred at a frequency of approximately one event per six crypts. All analyses were performed on crypts in the proximal segment of the duodenum.

Clone size was determined as the number of cells marked by a single fluorescent protein upon recombination of the *R26R-Confetti* allele. Cytoplasmic GFP intensity derived from the *Lgr5* knock-in allele allowed the identification of Lgr5^{hi} cells within a clone. Invariably, the identification of Lgr5^{hi} cells by cytoplasmic GFP was confirmed by their location between Paneth cells. The first Confetti-marked stem cells were observed 24 hr after Cre induction (Figure 4A). Most clones consisted of a single cell, of which 90% (34/38) could be identified as an Lgr5^{hi} cell located between Paneth cells (Figure 4B). Around 10% (5/43) of the marked stem cells had already undergone mitosis (Figure 4B).

After 2 days, most cells had divided at least once (Figures 4C and 4D). We scored 101 two-cell clones for the presence of Lgr5 ^{hi} cells. Of these, 54 clones contained two Lgr5 ^{hi} cells, 10 contained a single Lgr5^{hi} cell, and 37 contained no Lgr5^{hi} cells (Figure 4D). Alongside the 101 two-cell clones, there were a further 37 larger clones with mixed *Lgr5* expression, including one seven-cell clone containing no Lgr5^{hi} cells, and others with four cells all of which were Lgr5^{hi}. Apart from an overall expansion of clone size, this general pattern of behavior (broad size distribution and divergent fates) was maintained at day 3 with the largest clone having as many as 10 cells (Figures 4E and 4F).

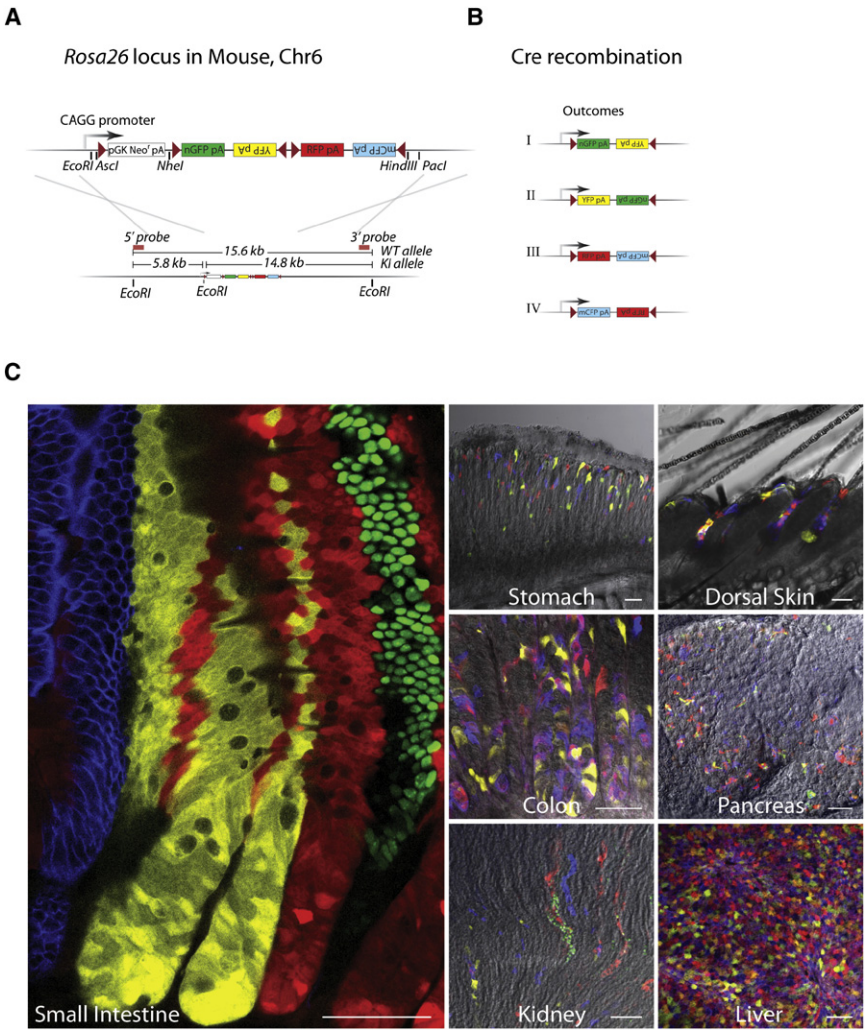

Figure 3. *R26R-Confetti*; a Stochastic Multicolor Cre-Reporter

(A) *R26R-Confetti* knock-in strategy. Brainbow2.1 encoding four fluorescent proteins (Livet et al., 2007) was inserted into the *Rosa26* locus. Upstream, the strong CAGG promoter, a LoxP site, and a neomycin resistance roadblock cassette were inserted.

(B) Upon cre activation, the neomycin roadblock is excised, while the brainbow2.1 recombines in a random fashion to four possible outcomes. GFP is nuclear, CFP is membrane associated, and the other two are cytoplasmic.

(C) The *R26R-Confetti* knock-in line is a stochastic multicolor Cre-reporter in multiple tissues. Scale bars: 50 μm, except for pancreas, kidney, and liver: 100 μm.

These results were indicative of the intestinal stem cells following seemingly divergent fates.

At later time points (day 7 and day 14), the rapid expansion and transfer of cells through the TA cell compartment to the villus made it challenging to reliably score their number. Therefore, we scored the number of Lgr5^{hi} cells in each clone at days 1, 2, 3, 7, and 14, while disregarding all other cell types within the clone. Thus, a ten-cell clone comprised of four Lgr5^{hi} cells and six Lgr5^{lo} cells translates to a clone of size 4, while a ten-cell clone in which all cells are Lgr5^{lo} was considered "extinct." With this definition, the size distribution of surviving clones is shown over the 14 day chase period (Figure 4G). The data reveal a steady increase in the average clone size that compensates for the ongoing extinction of clones. Indeed, by day 14, the largest clone contained as many as 12 Lgr5^{hi} cells, a figure approaching the 14 Lgr5^{hi} cell average found in duodenal crypts.

It was apparent that, even in the largest surviving clones, the labeled Lgr5^{hi} cells were largely grouped together suggesting that, despite their rapid turnover, mixing of cells at the crypt base was limited (Figure S2, Movie S1, and Movie S2). Furthermore, the morphology of these clones in the Lgr5^{hi} compartment was consistent with a lateral expansion around the circumference of the crypt base, whereas few, if any, cell divisions lead to clonal expansion through the base to the opposite side of the crypt.

Long-Term Lineage Tracing

In the second strategy, we aimed to mark all stem cells in crypts to document the drift toward clonality. The *Lgr5* gene is expressed at low levels and, as a consequence, the *Lgr5-EGFP-Ires-CreERT2* allele does not generate quantitative Cre activation upon a single tamoxifen induction. We therefore used the *R26R-Confetti* allele in conjunction with the *Ah-Cre* allele. The *Ah-Cre* transgene recombines LoxP sites efficiently in most cell types including the stem cells yet is inactive in the long-lived Paneth cells (Ireland et al., 2004). Nevertheless, within the Paneth cell compartment, old unmarked Paneth cells are replaced by marked precursor cells over time (Ireland et al., 2005). Clonal analysis was performed at various time points after Cre activation in 10-week-old *Ah-Cre*/*R26R-Confetti* mice, using "side-view" and "bottom-view" imaging of whole-mount intestine ("xy plane" and "xz plane," respectively; Figure 5A). Thus, the composition of many crypts could be captured in a single confocal image taken just above the crypt base, and for each crypt displayed as the biological equivalent of a "pie-chart." Analysis of the crypts in the time course provided visual snapshots of individual labeled domains of cells within crypts (Figure 5B). Using these "bottom-view" images, we were able to extract quantitative data from week 1 to week 30, documenting the drift toward clonality (Figure 5B).

Although only a small fraction of cells acquired the nuclear GFP label, 80% of the remaining cells were induced in approximately equal proportions, yellow:blue:red. At the earliest time point taken at 4 days post-labeling, the confocal section at the crypt base showed a striking, heterogeneous pattern of labeling (Figure 5B). At day 7, there was a significant expansion and

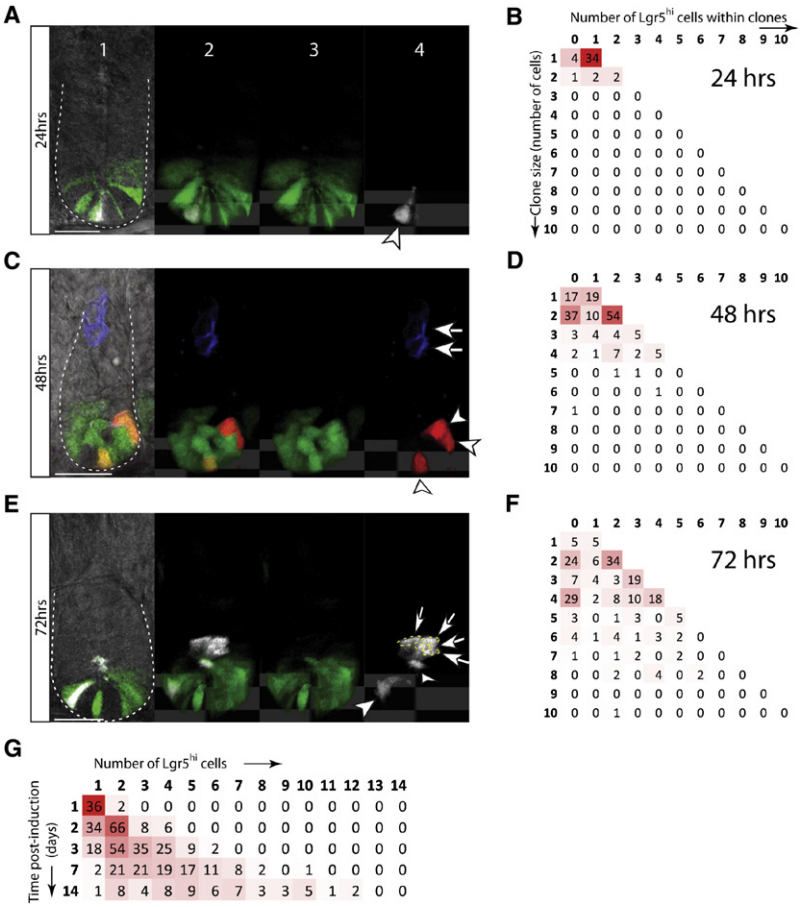

Figure 4. Short-Term Clonal Tracing Analysis of Individually Labeled Lgr5^{hi} Cells

(A) *R26R-Confetti* mice were crossed with *Lgr5-EGFP-Ires-CreERT2* mice. Tracing was sporadically induced in single Lgr5^{hi} cells (~1 Confetti color in 6 crypts). Cytosolic GFP marks the Lgr5^{hi} stem cell population. Panels from left to right: (1) single plane-2D image of crypt with one YFP (white, false color) labeled Lgr5^{hi} cell. Background is DIC image; (2) 3D reconstruction of the same crypt showing Lgr5^{hi} cells (green) and the traced cell (white); (3) same, but GFP only; (4) same but YFP only. Arrowheads point to Lgr5^{hi} cells within a clone, arrows point to TA cells within clone that lost Lgr5^{hi} activity.

(B) For 43 labeled clones, the total number of cells and numbers of Lgr5^{hi} cells were scored. The matrix indicates the absolute number of clones scored for each given clone size and given number of Lgr5^{hi} cells. Red hues represent relative frequencies of all scored events for given time point. 100% is red; 0% is white.

(C) As in (A), but after 48 hr of tracing. In this crypt, RFP (red) revealed a tracing event. The red clone expanded to three Lgr5^{hi} cells. By contrast, CFP (blue) revealed another tracing event in the same crypt, but where the clone lost *Lgr5* expression.

(D) As in (B), but after 48 hr of tracing.

(E) As in (A), but after 72 hr of tracing. One Lgr5^{hi} cell was labeled with YFP (white) and grown to a clone size of 6, of which two cells remained Lgr5^{hi}.

(F) As in (B), but after 72hr of tracing.

(G) Expansion of Lgr5^{hi} cell numbers over time within clones with at least one Lgr5^{hi} cell. The average size of these "surviving" clones gradually increases, yet the variability between individual clone sizes increases over time as well. Red hues represent relative frequency of Lgr5^{hi} cell numbers per time point. 100% is red; 0% is white.

Scale bars: 25 μm. See also Figure S2, Movie S1, and Movie S2.

coarsening of the labeled domains reflecting stem cell loss and lateral expansion of neighboring clones (Figure 5B). At later time points, we observed a continuing expansion of the average domain size alongside an ever-diminishing number of domains until crypts became fully labeled with one color (monochromatic) or fully unlabeled (Figure 5B). The first monochromatic crypts appeared as early as 2 weeks post-induction, whereas around 75% had become fully labeled at 2 months (Figure 5B). Although the drift toward monoclonality continued, we noted the presence—albeit rare—of oligo-clonal crypts even at 18 and 30 weeks post-labeling (Figure 5B, circles).

To describe quantitatively the drift toward clonality, we converted the sections from the crypt base into a labeled domain-size distribution (Figure 6A). Specifically, we divided the circumference into 16 equal parts ("sextadecals"), reflecting the typical number of TA cells in a section near, but above, the crypt base (Potten and Loeffler, 1990). This assignment related proportionately to the stem cell content of a clone. For example, if we found a labeled domain of size 4 sextadecals—i.e., covering one quarter of the crypt circumference—this translated to one quarter of the crypt base stem cells being labeled in that color. In this way, we could determine the labeled domain size distribution (Figure 6B) as well as the frequency of monochromatic crypts (Figure 6C) over the 30 week chase period.

On day 7, the domain size distribution was tilted toward smaller clone sizes with a peak around 3 to 4 sextadecals, i.e., clones covering 3/16 to 4/16 of the circumference (Figure 6B). At 2 weeks, the weight of the distribution was gradually shifting toward larger clone sizes (Figure 6B), with a small fraction of crypts (ca. 5%) already fully labeled (Figure 6C). At 4 weeks, the average domain covered around 8 sextadecals, the half-filled crypt, in partially labeled crypts (Figure 6B), whereas about 45% had become monochromatic (Figure 6C). This trend continued out to the latest time point at 30 weeks when almost all crypts were monochromatic. This behavior was consistent with competition between neighboring stem cells leading to ever fewer yet larger clones and a steady progression toward monoclonality. This phenomenon was age independent, as we observed the same drift toward clonality, when lineage tracing was initiated in 40-week-old mice (Figure S3).

Taken together, the short- and long-term clonal fate data rule out a model in which all Lgr5^{hi} cells are stem cells that segregate cell fate asymmetrically (Figures 4B, 4D, and 4F). Such a model would not be compatible with the previous observation—confirmed here—that crypts drift toward clonality (Griffiths et al., 1988; Winton et al., 1988). However, these early observations leave open the question of the functional homogeneity (i.e., equipotency) of the Lgr5^{hi} population. Indeed, the divergence of

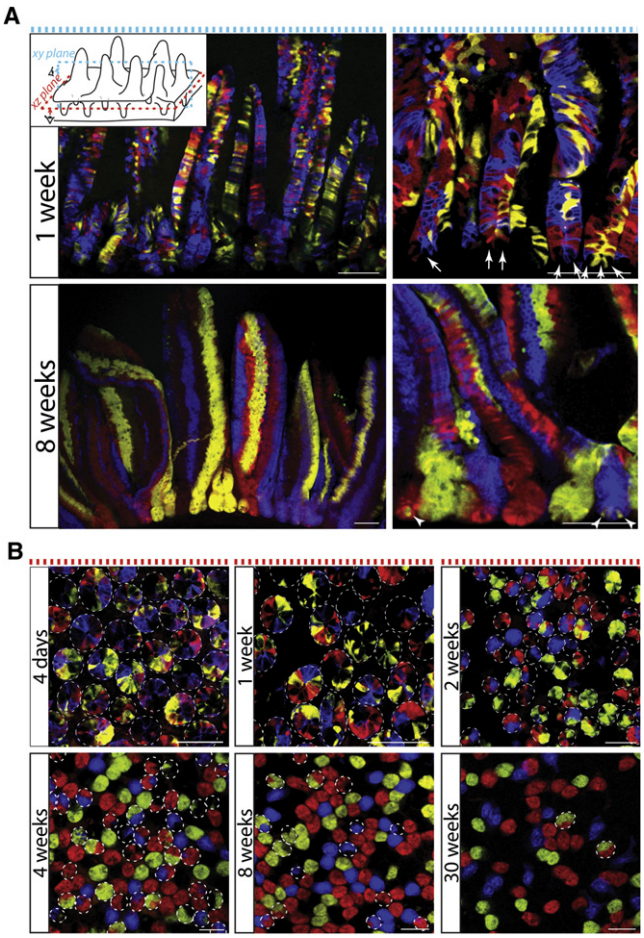

Figure 5. Long-Term Lineage Tracing

(A) *R26R-Confetti* mice were crossed with *Ah-Cre*. xy plane images are shown at 1 week and 8 weeks after cre induction. Left panels are overview images. Right panels zoom in on crypts. Over time, labeled cell domains expand whereas neighboring domains become extinct. Note that Paneth cells are long-lived and can reveal the "clonal history" of a crypt when derived from a clone that is extinct at the time of analysis. Inset: schematic representation of small intestine, indicating the two sectioning planes used for the analysis.

(B) xz-plane images of small intestine after *R26R-Confetti* activation reveal drift toward clonality over time. Nonclonal crypts are marked with a white-dashed circle.

Scale bars: 100 μm. See also Figure S3.

clone fate seen in short-term lineage tracing and the progression to monoclonality at longer times could be both accommodated within two very different frameworks. In the *hierarchical model* (1), the Lgr5^{hi} cell compartment may be functionally heterogeneous with progenitor cells of limited proliferative potential supported by a single "dominant" stem cell following a strict pattern of invariant asymmetry such as proposed previously. Alternatively, in the *stochastic model* (2), tissue is maintained by an equipotent Lgr5^{hi} stem cell population following a pattern of population asymmetry in which stem cell loss is compensated by symmetric self-renewal of a neighboring stem cell.

At present, no marker or unique location has been identified that would distinguish a "dominant" Lgr5^{hi} stem cell in the *hierarchical model* from its Lgr5^{hi} progeny. Although, the validity of the model can thus not be addressed directly, several indirect conclusions can be drawn. First, for the model to be valid, the dominant stem cell has to be Lgr5^{hi}, given that *Lgr5*-based tracing eventually leads to the marking of entire crypts. Second, the dominant stem cell has to divide in a strictly asymmetric fashion as a crypt can only harbor a single such cell. Third, because the kinetics of drift toward clonality differs from crypt to crypt, the dominant Lgr5^{hi} stem cell should yield Lgr5^{hi} progenitors, which can occur as relatively long-lived Lgr5^{hi} cells (which persist for many months) but should also occur as short-lived Lgr5^{hi} cells that disappear within days. Both long- and short-lived Lgr5^{hi} progenitors should still be multipotent, again based on our previous tracing data (Barker et al., 2007).

In the *stochastic model* the situation is much less complicated. Only one type of Lgr5^{hi} cell exists, 14 per crypt, all endowed with the potential for long-term stemness. Cell fate is determined after division of the Lgr5^{hi} stem cell, potentially by competition for available niche space at the crypt base. Thus, homeostasis is obtained by neutral competition between equal stem cells and occurs at the population level. To evaluate the possibility that the stochastic model indeed underlies the homeostatic self-renewal in crypts, we subjected our quantitative short- and long-term tracing data to a theoretical analysis.

Mathematical Analysis of Short-Term Clonal Evolution Shows that Stem Cells Follow Neutral Drift Dynamics

In general, the ability to maintain tissue in long-term homeostasis places significant constraints on the properties of a stem cell population. In particular, it leaves open two patterns of stem cell fate: invariant asymmetry in which every stem cell division results in asymmetric fate (as exemplified by the hierarchical model), and population asymmetry in which the balance between self-renewal and differentiation is achieved on a population basis (as exemplified by the stochastic model) (Watt and Hogan, 2000). For the latter, because the size of the intestinal stem cell compartment remains roughly constant over time, it follows that balance of stem cell fate in crypts must follow from external regulation: the tissue responds to the loss of a nearby stem cell by symmetric cell division or vice versa. As a result, stem cells follow a stochastic pattern of behavior known as "neutral drift dynamics." If, by chance, the last stem cell in a clone is lost, that particular clone becomes extinct. As a consequence, crypts inevitably drift toward clonality in the stochastic model. Evidence for population asymmetry and neutral drift dynamics has been reported recently for stem cells in mammalian testis (Klein et al., 2010). Two of us (A.M.K. and B.D.S.) have provided the theoretical underpinning for a study comparable to that of Klein et al. on intestinal crypt-villus dynamics (Lopez-Garcia et al., 2010). Both of these studies relied upon long-term lineage tracing from which the "trails" of differentiating spermatocytes, and the migration streams of intestinal cells on the villi, were used to infer indirectly the dynamics of the underlying stem cell compartments.

With access to clonal fate data at single stem cell resolution, the present study allowed for a critical, direct analysis of the dynamics of the intestinal stem cell population. From the two

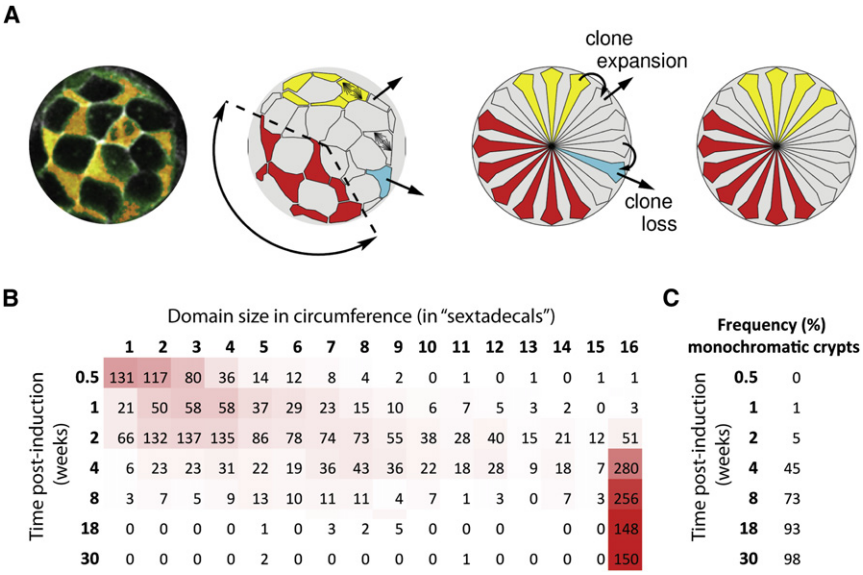

Figure 6. Progression toward Monoclonality

(A) Schematic representation of the translation from actual data to quantitation of labeled domain sizes. Left panel shows the crypt base with Lgr5^{hi} cells in false color red, *Lgr5* expression in green, and E-cadherin-mCFP in white. Second panel is a schematic representation of the crypt base, in which three hypothetical labeled cell domains were visualized in red, yellow, and blue. The red domain shows seven labeled cells and encompasses 7/16 of the crypt base circumference. Two mitoses are shown; the first leads to the displacement and loss of the blue single-cell clone, and the second leads to the displacement of an unlabeled cell and the expansion of the yellow clone. The third panel illustrates the segregation of the crypt base into 16 equally spaced segments (sextadecals) corresponding approximately to the cellular composition of the crypt base stem cells. The process of Lgr5^{hi} cell displacement following the symmetric duplication of a neighboring Lgr5^{hi} cell is shown for two clones, with the outcome shown in the final panel.

(B) The matrix indicates the absolute number of clones scored for each given domain size at each time point post-induction. Red hues represent relative frequencies of all scored domain sizes per time point. 100% is red; 0% is white.

(C) Frequencies of monochromatic crypts after given time points post-induction.

studies mentioned above, several generic and robust features of neutral drift dynamics have emerged. First, after an initial transient evolution, the clone size distribution was predicted to acquire "scaling" behavior: Formally, denoting as P_n (t) the fraction of surviving clones which host n (>1) Lgr5^{hi} cells at a time t post-induction, we can define a cumulative size distribution, $C_n(t) = 1 - \sum_{m=1}^{n} P_m(t)$, i.e., $C_n(t)$ simply records the chance of finding a clone with *more than n* stem cells after a time t. For the latter, "scaling" implies that the cumulative size distribution takes the form (Supplemental Information—Theory),

$$C_n(t) = F(n/\langle n(t)\rangle), \quad (1)$$

where $\langle n(t)\rangle$ denotes the average number of stem cells in a surviving clone, and F is the "scaling function." From (1), it follows that, when C_n (t) is plotted against $n/\langle n(t)\rangle$, the entire family of size distributions at different times, t, collapses onto a single curve. The scaling function, F, is "universal," independent of stem cell number and rate of loss or division, etc., and dependent only on the coordination of stem cells in tissue (see below). In crypts, because clone size cannot grow indefinitely, scaling behavior will be lost when crypts become monoclonal (Supplemental Information—Theory).

By contrast, if homeostasis relies upon a stem cell hierarchy, clones derived from the dominant stem cell would increase steadily in size, whereas those derived from shorter-lived Lgr5^{hi} cells would exhibit limited growth followed by loss. Significantly, the mixture of these two behaviors cannot lead to scaling (Klein et al., 2010). The growth, $\langle n(t)\rangle$, and form of F, offer further insight into the pattern of stem cell fate. If stem cells are organized into a one-dimensional arrangement, with cell replacement effected by neighboring stem cells, then the average size of surviving clones is predicted to acquire a square root time dependence, $\langle n(t)\rangle \approx \sqrt{\pi\lambda t}$, with λ as the stem cell replacement rate, and the scaling function taking the form (Supplemental Information—Theory; Bramson and Griffeath, 1980),

$$F(x) = \exp(-\pi x^2/4). \quad (2)$$

Referring to Figures 7A and 7B, we indeed found that the cumulative clone size distribution from the short-term clonal assay showed a rapid convergence onto scaling behavior, whereas the average clone size followed a square root growth over the same period. Such scaling behavior is consistent with equipotency of all Lgr5^{hi} cells, thereby arguing against the hierarchical model. Furthermore, the coincidence of the data with the universal (parameter-free) scaling function (2) further established that intestinal stem cells follow a pattern of neutral drift dynamics in which stem cell multiplication is compensated by the loss of neighboring stem cells. This leads to a lateral clonal expansion around the one-dimensional circumference defined by the crypt base (Figure 6A) and consistent with the images obtained from whole mounts (Figure 5B). A fit of the predicted average clone size $\langle n(t)\rangle$ (Figure 7A, solid line, Supplemental Information—Theory) to the experimental data over the 14 day chase period (Figure 7A, points) revealed a stem cell replacement rate of 0.74 ± 0.04/day, a figure comparable with the cell division rate of the stem cells. As a result of this coincidence, we can conclude that, if asymmetric stem cell divisions take place at all, they make a minimal contribution to tissue homeostasis.

From the inferred rate of stem cell loss, we can use neutral drift dynamics to predict the long-term evolution of the average clone size and survival probability (Figures 7C and 7D). With this result in hand, a further comparison of the clone size distribution with a more detailed analysis that includes the approach to scaling (Supplemental Information—Theory) revealed an

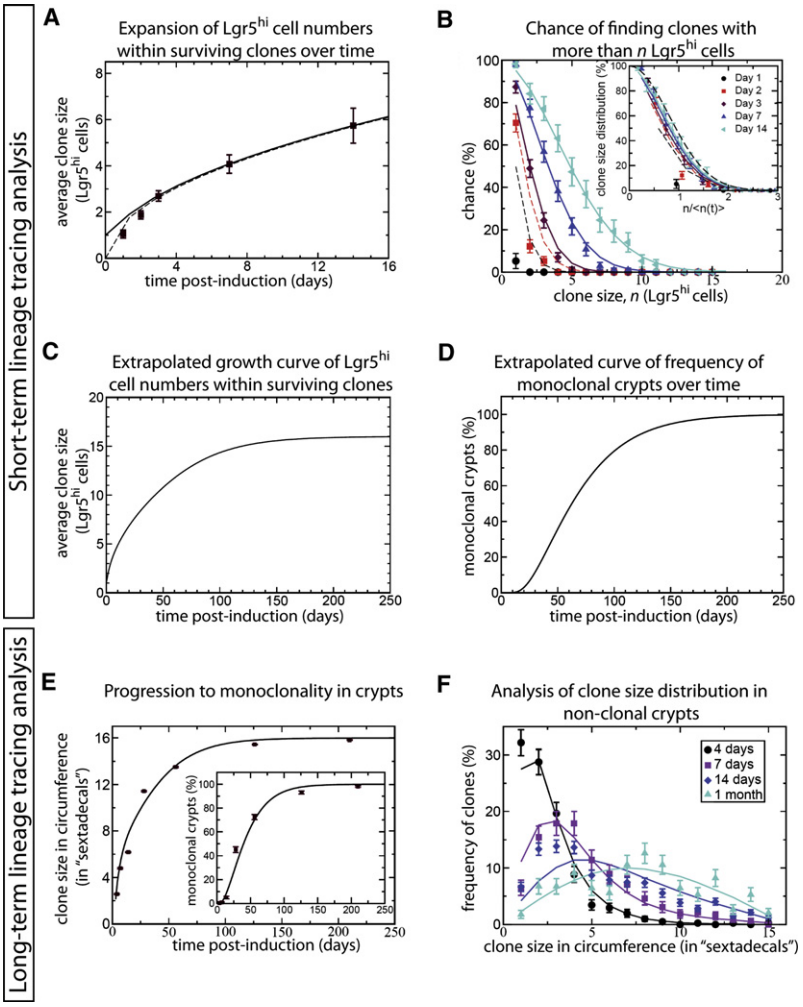

Figure 7. Lgr5^{hi} Cells Follow Neutral Drift Dynamics

(A) A fit of the average number of Lgr5^{hi} cells within surviving clones as predicted by the stochastic model of neutral drift dynamics (solid line, Supplemental Information—Theory) to the experimental data (points, see Figure 4G) leads to a stem cell loss rate of 0.74 ± 0.4/day. The dashed curve shows a simple square root time dependence, which provides an increasing good approximation to the exact result. Error bars denote the standard error of the proportion.

(B) Cumulative clone size distribution, $C_n(t)$, i.e., the chance of finding a surviving clone with more than n stem cells, as measured by the Lgr5^{hi} content within surviving clones. The lines show the size distribution as predicted by neutral drift dynamics with the stem cell loss rate fixed by the fit in (A) (Supplemental Information—Theory) while the points show experimental data from days 1, 2, 3, 7, and 14 (Figure 4G). Inset: at these early times, theory predicts that, if stem cell self-renewal follows from population asymmetry (the stochastic model), the cumulative clone size distribution, $C_n(t)$, should collapse onto a universal scaling curve when plotted as a function of $n/ < n(t) >$, where $< n(t) >$ denotes the average size of the surviving clones. Such behavior is recapitulated by the experimental data, with the dashed curve representing the universal scaling function (2). Error bars denote the standard error of the proportion.

(C) The growth curve over time of Lgr5^{hi} stem cell number within surviving clones as predicted by neutral drift dynamics with the stem cell loss rate of 0.74/day (obtained from Figure 7A) and 16 stem cells per crypt.

(D) The corresponding frequency of monoclonal crypts over time as a percentage of surviving clones as predicted by neutral drift dynamics.

(E) Average size of labeled cell domains following long-term fate mapping of intestinal stem cells. Once again, with 16 stem cells per crypt, and an average stem cell loss rate of 0.74/day, the line shows the prediction following neutral drift dynamics (Supplemental Information—Theory) while the points are obtained from experiment at 4, 7, 14, 28, 61, 126, and 210 days post-induction (Figures 6B and 6C). The corresponding frequency of monochromatic crypts (in which all progenitor cells are labeled with the same color) is shown in the inset. Error bars denote the standard error of the proportion.

(F) Variability in clone size for partially labeled crypts at 4, 7, 14, and 28 days post-induction. The predictions made by neutral drift dynamics (lines, Supplemental Information—Theory) match closely with the experimental data (points, Figure 6B). Error bars denote the standard error of the proportion.

See also Figure S4.

excellent agreement of theory (Figure 7B, lines) with experiment at intermediate times (Figure 7B, points).

Long-Term Clonal Evolution, Coarsening, and the Progression to Monoclonality

The long-term lineage tracing data provided a vivid demonstration of the ''coarsening'' phenomenon (i.e., the drift toward ever fewer, yet larger clones) predicted by neutral drift dynamics. It also presented an opportunity to study quantitatively the progression to monoclonality. The size distribution of contiguous labeled patches of stem cells generated in the *R26R-Confetti* system provided a signature of neutral drift dynamics, which can be compared to theory—a straightforward generalization of the clonal dynamics considered in the previous section to a multicolor mosaic system. Although the clone dynamics relates to an, as yet, unsolved problem in nonequilibrium statistical physics—the theory of a ''coalescing random walk'' (Ben-Naim et al., 1996; Krapivsky and Ben-Naim, 1997; Wu, 1982)—the evolution could be generated straightforwardly by computer simulation, and the results compared with experiment (Figure S4 and Supplemental Information—Theory).

To extract quantitative insights from the experimental data, we required one further parameter, the number of stem cells in the crypt. Duodenal crypts harbor 14 ± 2 Lgr5^{hi} cells per crypt. In the following, we have assumed a figure of 16 stem cells per crypt to match the average number of TA cells in a crypt section near the base. However, within a relatively narrow range of 14–18, a variable stem cell number would not significantly influence the quality of the fits discussed below. Taking the same stem cell loss rate from the short-term clonal analysis, Figure 7E shows a favorable agreement of neutral drift dynamics (solid line) with the measured average clone size (points) as well as the

monochromatic crypt fraction (Figure 7E, inset). In particular, the figure shows that, by 2 months, approximately 75% of the crypts became monoclonal (Figure 7A, inset).

As with the short-term clonal assay, the average size dependence represented just one facet of a rich data set associated with the full clone size distribution. With the same two parameters in hand, the stem cell loss rate and stem cell number, an analysis of the size distribution showed an equally favorable agreement (solid lines) with the experimental data (points) at 4, 7, 14, and 28 days post-labeling (Figure 7F). At longer times, the data were fully consistent with theory, but the numbers of nonclonal crypts had become too low to reach statistical significance.

DISCUSSION

We have studied how homeostasis of intestinal stem cell compartments is accomplished by following the fates of clonally labeled Lgr5^{hi} cells. Although we cannot rigorously rule out the hierarchical model (as long as the model allows unlimited complexity in the cellular composition of individual crypts), our data favor the stochastic model based on the following arguments: The stochastic model is the simplest model, as it postulates the existence of only a single type of Lgr5^{hi} cell. The model endows every Lgr5^{hi} cell with potential stemness, which agrees with our observations that the majority of Lgr5^{hi} cells can establish long-lived intestinal organoids. By contrast, the hierarchical model would endow only 1 of 14 Lgr5^{hi} cells with stemness. And importantly, the stochastic model is in excellent agreement with both the early-tracing data (Figure 4) and the drift-toward-clonality data (Figure 6).

It has recently been reported that Lgr5^{hi} cells orient their spindle along the apico-basal axis (Quyn et al., 2010). This may herald the generation of unequal daughter cells because, after division, the individual daughters may find themselves in different environments. This occurs in the *Drosophila* testis, where the germ stem cell divides perpendicular to a niche structure, termed the hub. This ensures that one cell will continue as a stem cell attached to the hub, while the other differentiates into a gonial blast (Yamashita et al., 2003). Similarly, germ stem cells and escort stem cells in the *Drosophila* ovary divide away from the niche cells of the ovary, the cap cells (Deng and Lin, 1997). Such an orientation ensures the generation of the downstream daughter (the prospective cystoblast) and the generation of a new cap cell-associated stem cell (Fuller and Spradling, 2007). All Lgr5^{hi} cells span the epithelial sheet, from basal lamina to apical lumen. Their flanks uniformly touch Paneth cells. Thus, even though the spindle is oriented perpendicular to the epithelial sheet, the daughter cells do not end up in divergent locations. We propose that spindle orientation in Lgr5^{hi} cells results from spatial constraints in these flattened polarized cells.

A stochastic model involving neutral competition (for instance for niche space) between equal stem cells and leading to neutral drift dynamics may be operative in other mammalian tissues. Indeed, the stochastic model generates features of homeostatic self-renewal that, without detailed scrutiny, would appear to be exponents of the hierarchical model. For instance, the drift-toward-clonality intuitively implies the "predetermined" presence of a single long-lived stem cell, the central characteristic of the hierarchical model. Yet, our quantitative analysis shows that it is also the inevitable outcome of the stochastic model. Further, intuitively the wide diversity in life span of progenitors would be indicative of the existence of a variety of long-lived and short-lived progenitors, another feature of the hierarchical model. Yet, the stochastic model of equal stem cells inevitably generates a similar richness in life span.

For at least two cases, the long-lived keratinocyte progenitor in the basal layer of the epidermis (Clayton et al., 2007) and the germline stem cells in mammalian testis (Klein et al., 2010), it has been shown that stochastic outcome of the division of a single type of potentially long-lived progenitor maintains tissue homeostasis. In both cases, only a single type of differentiated cell is generated and one may therefore argue that the epidermis and testis don't represent examples of multipotent stem cell-driven self-renewal. Although technically challenging, it would be of great interest to perform clonal tracing in "classic" stem cell models such as the bone marrow. More examples may be unveiled in which homeostasis is obtained at the population level by competition between equal stem cells, rather than at the single stem cell level by strictly asymmetric cell divisions.

EXPERIMENTAL PROCEDURES

Mice

E-cadherin-mCFP mice were generated using the construct in Figure 1A. The neomycin selection cassette was excised in vivo by crossing the mice with the PGK-Cre mouse strain. For *E-cadherin-mCFP* genotyping PCR primers, see Table S1. *E-cadherin-mCFP* mice were bred with *Lgr5-EGFP-Ires-CreERT2* mice. Double heterozygous mice of 10 weeks were used for experiments. *R26R-Confetti* mice were generated using the construct in Figure 3A. For the brainbow 2.1 construct, refer to Livet et al. (2007). See Table S1 for the *R26R-Confetti* genotyping PCR primers. *R26R-Confetti* mice were crossed with *Lgr5-EGFP-Ires-CreERT2* or with *Ah-Cre* mice. Cre induction: 10 week-old mice were injected with 5 mg tamoxifen (single injection) or β-naphtoflavone (3× 100 mg in one day), respectively.

Tissue Preparation for Confocal Analysis

For semi-thick sectioning of near-native tissue, organs were fixed in 4% paraformaldehyde at room temperature for 20 min and washed in cold PBS. 1 cm^2 of intestinal wall was put in a mold. Four percent low melting point agarose (40°C) was added and allowed to cool on ice. Once solid, a vibrating microtome (HM650, Microm) was used to make semi-thick sections (150 μm) (velocity: 1 mm/s, frequency: 65 Hz, amplitude: 0.9 mm). Sections were directly embedded in Vectashield (Vector Laboratories).

FACS Analysis of Lgr5 Populations and In Vitro Culture

Lgr5$^+$ cells were FACS analyzed as previously described (van der Flier et al., 2009). Crypts were dissociated with TrypLE express (Invitrogen) with 2000 U/ml DNase (Sigma) for 30 min at 37°C. Dissociated cells were passed through 20 μm cell strainer (Celltrix) and washed with PBS. Cells were stained with CD24-PE antibody (eBioscience) and Epcam-APC antibody (eBioscience) for 15 min at 4°C and analyzed by MoFlo (DakoCytomation). Viable epithelial single-cells or doublets were gated by forward scatter, side scatter and pulse-width parameter, and negative staining for propidium iodide. Sorted cells were embedded in Matrigel. Crypt culture medium (advanced DMEM/F12 supplemented with Penicillin/Streptomycin, 10 mM HEPES, Glutamax, 1x N2, 1x B27 [Invitrogen], and 1 μM N-acetylcysteine [Sigma] containing 50 ng/ml EGF, 100 ng/ml noggin, 1 μg/ml R-spondin) was overlaid. Y-27632 (10 μM) was included for the first 2 days to avoid anoikis. Growth factors were added every other day and the entire medium was changed every 4 days. In three

independent experiments, organoid formation was analyzed 7 days after plating.

Microscope Equipment

Images were acquired using a Leica Sp5 AOBS confocal microscope (Mannheim, Germany) equipped with the following lenses: 10× (HCX PL APO CS NA0.40) dry objective; 20× (HCX PL FLUOTAR L NA0.40) dry objective; 40× (HCX PL APO NA0.85) dry objective; and a 63× (HCX PL APO NA1.30) glycerol objective.

SUPPLEMENTAL INFORMATION

Supplemental Information includes Extended Experimental Procedures, four figures, one table, and two movies and can be found with this article online at doi:10.1016/j.cell.2010.09.016.

ACKNOWLEDGMENTS

We thank Stieneke van den Brink, Jeroen Korving, and the Hubrecht Imaging Center for technical assistance. We thank J. Lichtman for the Brainbow2.1 cassette. A.M.K. and B.D.S. acknowledge insightful discussions with Douglas Winton and Carlos Lopez-Garcia.

Received: July 15, 2010
Revised: September 7, 2010
Accepted: September 10, 2010
Published: September 30, 2010

REFERENCES

Barker, N., van Es, J.H., Kuipers, J., Kujala, P., van den Born, M., Cozijnsen, M., Haegebarth, A., Korving, J., Begthel, H., Peters, P.J., et al. (2007). Identification of stem cells in small intestine and colon by marker gene Lgr5. Nature *449*, 1003–1007.

Barker, N., Huch, M., Kujala, P., van de Wetering, M., Snippert, H.J., van Es, J.H., Sato, T., Stange, D.E., Begthel, H., van den Born, M., et al. (2010). Lgr5(+ve) stem cells drive self-renewal in the stomach and build long-lived gastric units in vitro. Cell Stem Cell *6*, 25–36.

Ben-Naim, E., Frachebourg, L., and Krapivsky, P.L. (1996). Coarsening and persistence in the voter model. Phys. Rev. E Stat. Phys. Plasmas Fluids Relat. Interdiscip. Topics *53*, 3078–3087.

Bramson, M., and Griffeath, D. (1980). Asymptotics for interacting particle systems on Zd. Probab. Theory Relat. Fields *53*, 183–196.

Cheng, H., and Leblond, C.P. (1974a). Origin, differentiation and renewal of the four main epithelial cell types in the mouse small intestine. I. Columnar cell. Am. J. Anat. *141*, 461–479.

Cheng, H., and Leblond, C.P. (1974b). Origin, differentiation and renewal of the four main epithelial cell types in the mouse small intestine. V. Unitarian Theory of the origin of the four epithelial cell types. Am. J. Anat. *141*, 537–561.

Clayton, E., Doupe, D.P., Klein, A.M., Winton, D.J., Simons, B.D., and Jones, P.H. (2007). A single type of progenitor cell maintains normal epidermis. Nature *446*, 185–189.

Cowan, C.R., and Hyman, A.A. (2004). Asymmetric cell division in C. elegans: cortical polarity and spindle positioning. Annu. Rev. Cell Dev. Biol. *20*, 427–453.

Deng, W., and Lin, H. (1997). Spectrosomes and fusomes anchor mitotic spindles during asymmetric germ cell divisions and facilitate the formation of a polarized microtubule array for oocyte specification in Drosophila. Dev. Biol. *189*, 79–94.

Fuller, M.T., and Spradling, A.C. (2007). Male and female Drosophila germline stem cells: two versions of immortality. Science *316*, 402–404.

Griffiths, D.F., Davies, S.J., Williams, D., Williams, G.T., and Williams, E.D. (1988). Demonstration of somatic mutation and colonic crypt clonality by X-linked enzyme histochemistry. Nature *333*, 461–463.

He, X.C., Zhang, J., Tong, W.G., Tawfik, O., Ross, J., Scoville, D.H., Tian, Q., Zeng, X., He, X., Wiedemann, L.M., et al. (2004). BMP signaling inhibits intestinal stem cell self-renewal through suppression of Wnt-beta-catenin signaling. Nat. Genet. *36*, 1117–1121.

He, X.C., Yin, T., Grindley, J.C., Tian, Q., Sato, T., Tao, W.A., Dirisina, R., Porter-Westpfahl, K.S., Hembree, M., Johnson, T., et al. (2007). PTEN-deficient intestinal stem cells initiate intestinal polyposis. Nat. Genet. *39*, 189–198.

Ireland, H., Kemp, R., Houghton, C., Howard, L., Clarke, A.R., Sansom, O.J., and Winton, D.J. (2004). Inducible Cre-mediated control of gene expression in the murine gastrointestinal tract: effect of loss of beta-catenin. Gastroenterology *126*, 1236–1246.

Ireland, H., Houghton, C., Howard, L., and Winton, D.J. (2005). Cellular inheritance of a Cre-activated reporter gene to determine Paneth cell longevity in the murine small intestine. Dev. Dyn. *233*, 1332–1336.

Jaks, V., Barker, N., Kasper, M., van Es, J.H., Snippert, H.J., Clevers, H., and Toftgard, R. (2008). Lgr5 marks cycling, yet long-lived, hair follicle stem cells. Nat. Genet. *40*, 1291–1299.

Klein, A.M., Nakagawa, T., Ichikawa, R., Yoshida, S., and Simons, B.D. (2010). Mouse germ line stem cells undergo stochastic turnover. Cell Stem Cell *7*, 214–224.

Krapivsky, P.L., and Ben-Naim, E. (1997). Domain statistics in coarsening systems. Phys. Rev. E Stat. Phys. Plasmas Fluids Relat. Interdiscip. Topics *56*, 3788–3798.

Li, L., and Clevers, H. (2010). Coexistence of quiescent and active adult stem cells in mammals. Science *327*, 542–545.

Livet, J., Weissman, T.A., Kang, H., Draft, R.W., Lu, J., Bennis, R.A., Sanes, J.R., and Lichtman, J.W. (2007). Transgenic strategies for combinatorial expression of fluorescent proteins in the nervous system. Nature *450*, 56–62.

Lopez-Garcia, C., Klein, A.M., Simons, B.D., and Winton, D.J. (2010). Intestinal stem cell replacement follows a neutral drift. Science, in press.

Marshman, E., Booth, C., and Potten, C.S. (2002). The intestinal epithelial stem cell. Bioessays *24*, 91–98.

Morrison, S.J., and Spradling, A.C. (2008). Stem cells and niches: mechanisms that promote stem cell maintenance throughout life. Cell *132*, 598–611.

Neumuller, R.A., and Knoblich, J.A. (2009). Dividing cellular asymmetry: asymmetric cell division and its implications for stem cells and cancer. Genes Dev. *23*, 2675–2699.

Potten, C.S., and Loeffler, M. (1990). Stem cells: attributes, cycles, spirals, pitfalls and uncertainties. Lessons for and from the crypt. Development *110*, 1001–1020.

Potten, C.S., Kovacs, L., and Hamilton, E. (1974). Continuous labelling studies on mouse skin and intestine. Cell Tissue Kinet. *7*, 271–283.

Potten, C.S., Booth, C., Tudor, G.L., Booth, D., Brady, G., Hurley, P., Ashton, G., Clarke, R., Sakakibara, S., and Okano, H. (2003). Identification of a putative intestinal stem cell and early lineage marker; musashi-1. Differentiation *71*, 28–41.

Quyn, A.J., Appleton, P.L., Carey, F.A., Steele, R.J., Barker, N., Clevers, H., Ridgway, R.A., Sansom, O.J., and Nathke, I.S. (2010). Spindle orientation bias in gut epithelial stem cell compartments is lost in precancerous tissue. Cell Stem Cell *6*, 175–181.

Sangiorgi, E., and Capecchi, M.R. (2008). Bmi1 is expressed in vivo in intestinal stem cells. Nat. Genet. *40*, 915–920.

Sato, T., Vries, R.G., Snippert, H.J., van de Wetering, M., Barker, N., Stange, D.E., van Es, J.H., Abo, A., Kujala, P., Peters, P.J., et al. (2009). Single Lgr5 stem cells build crypt-villus structures in vitro without a mesenchymal niche. Nature *459*, 262–265.

Snippert, H.J., van Es, J.H., van den Born, M., Begthel, H., Stange, D.E., Barker, N., and Clevers, H. (2009). Prominin-1/CD133 marks stem cells and early progenitors in mouse small intestine. Gastroenterology *136*, 2187–2194.

Snippert, H.J., Haegebarth, A., Kasper, M., Jaks, V., van Es, J.H., Barker, N., van de Wetering, M., van den Born, M., Begthel, H., Vries, R.G., et al. (2010).

Lgr6 marks stem cells in the hair follicle that generate all cell lineages of the skin. Science *327*, 1385–1389.

van der Flier, L.G., and Clevers, H. (2009). Stem cells, self-renewal, and differentiation in the intestinal epithelium. Annu. Rev. Physiol. *71*, 241–260.

van der Flier, L.G., van Gijn, M.E., Hatzis, P., Kujala, P., Haegebarth, A., Stange, D.E., Begthel, H., van den Born, M., Guryev, V., Oving, I., et al. (2009). Transcription factor achaete scute-like 2 controls intestinal stem cell fate. Cell *136*, 903–912.

Watt, F.M., and Hogan, B.L. (2000). Out of Eden: stem cells and their niches. Science *287*, 1427–1430.

Winton, D.J., and Ponder, B.A. (1990). Stem-cell organization in mouse small intestine. Proc. Biol. Sci. *241*, 13–18.

Winton, D.J., Blount, M.A., and Ponder, B.A. (1988). A clonal marker induced by mutation in mouse intestinal epithelium. Nature *333*, 463–466.

Wu, F.Y. (1982). The Potts model. Rev. Mod. Phys. *54*, 235–268.

Yamashita, Y.M., Jones, D.L., and Fuller, M.T. (2003). Orientation of asymmetric stem cell division by the APC tumor suppressor and centrosome. Science *301*, 1547–1550.

Zhu, L., Gibson, P., Currle, D.S., Tong, Y., Richardson, R.J., Bayazitov, I.T., Poppleton, H., Zakharenko, S., Ellison, D.W., and Gilbertson, R.J. (2009). Prominin 1 marks intestinal stem cells that are susceptible to neoplastic transformation. Nature *457*, 603–607.